Dielectric functions and optical bandgaps of high-*K* dielectrics for metal-oxide-semiconductor field-effect transistors by far ultraviolet spectroscopic ellipsometry

Seung-Gu Lim,[a] Stas Kriventsov, and Thomas N. Jackson
Center for Thin Film Devices, and Electronic Materials and Processing Research Laboratory, The Pennsylvania State University 121 EE East, University Park, Pennsylvania 16802

J. H. Haeni and D. G. Schlom
Department of Materials Science and Engineering, The Pennsylvania State University, 108 MRI Building, Research Park, Pennsylvania 16803-6602

A. M. Balbashov
Moscow Power Engineering Institute, Krasnokazarmennaya 14, 111250 Moscow, Russia

R. Uecker and P. Reiche
Institute of Crystal Growth, Rudower Chaussee 6, D-12489 Berlin, Germany

J. L. Freeouf
Oregon Graduate Institute and Interface Studies Inc., 672 N. W. Autumn Creek Way M202, Beaverton, Oregon 97006

G. Lucovsky
Department of Physics, North Carolina State University, Raleigh, North Carolina 27695-8202

(Received 21 August 2001; accepted for publication 9 January 2002)

A far ultraviolet (UV) spectroscopic ellipsometer system working up to 9 eV has been developed, and applied to characterize high-*K*-dielectric materials. These materials have been gaining greater attention as possible substitutes for SiO_2 as gate dielectrics in aggressively scaled silicon devices. The optical properties of four representative high-*K* bulk crystalline dielectrics, $LaAlO_3$, Y_2O_3-stabilized HfO_2 $(Y_2O_3)_{0.15}$–$(HfO_2)_{0.85}$, $GdScO_3$, and $SmScO_3$, were investigated with far UV spectroscopic ellipsometry and visible-near UV optical transmission measurements. Optical dielectric functions and optical band gap energies for these materials are obtained from these studies. The spectroscopic data have been interpreted in terms of a universal electronic structure energy scheme developed form *ab initio* quantum chemical calculations. The spectroscopic data and results provide information that is needed to select viable alternative dielectric candidate materials with adequate band gaps, and conduction and valence band offset energies for this application, and additionally to provide an optical metrology for gate dielectric films on silicon substrates. © *2002 American Institute of Physics.* [DOI: 10.1063/1.1456246]

I. INTRODUCTION

SiO_2 has long been the gate dielectric material of choice for silicon device applications due to its excellent material and interface properties including: (i) device-quality films that can be grown directly on silicon; (ii) a large energy band gap (~9 eV);[1] (iii) relatively large conduction and valence band offset energies with respect to Si (~3.2 and 4.5 eV, respectively); (iv) high effective electrical resistivity (10^{15}–10^{17} Ω cm), (v) excellent dielectric breakdown strength ($>10^7$ V/cm); (vi) low bulk and interface defect densities, $<10^{16}$ cm^{-3} and $<10^{11}$ cm^{-2}, respectively; and (vii) excellent thermal stability in contact with crystalline Si.[2] However, the relatively low dielectric constant ($K=3.9$) limits its use in transistors as gate lengths continue to shrink below 50 nm.[2,3] These studies show that device performance is limited by the tunneling leakage current through the ultra-thin gate oxides, <2 nm, required for devices with these aggressively scaled gate lengths. Recently, the possible use of high-*K* oxides containing transition metal or rare earth elements, including ternary silicate and aluminate phases, as an alternative gate dielectric has received considerable attention. This is important because devices with high-*K* gate dielectrics have the potential to provide comparable device performance with a much thicker dielectric layer, thereby reducing significantly the tunneling leakage currents. In a comprehensive study of essentially all possible elemental and multicomponent oxides by a thermodynamic approach, a number of high-*K* gate dielectric candidates with good silicon compatibility have been identified.[4–7] This was based solely on solid-phase stability and has recently been modified to include gaseous phases as well.[8]

Four silicon-compatible high-*K* bulk dielectrics, $LaAlO_3$, Y_2O_3-stablized HfO_2 $((Y_2O_3)_{0.15}(HfO_2)_{0.85})$, $GdScO_3$, and $SmScO_3$ have emerged from the studies in Refs. 4–7, and in this article the optical properties of these

[a]Author to whom correspondence should be addressed; electronic mail: sxl179@psu.edu

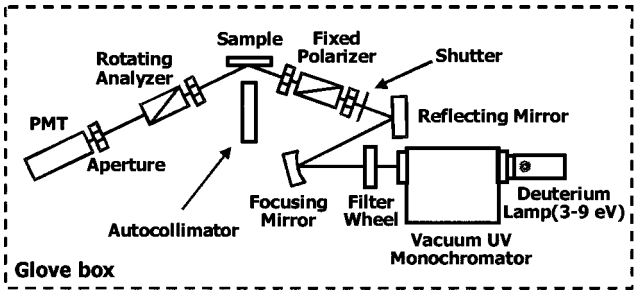

FIG. 1. Schematic of far UV spectroscopic ellipsometer.

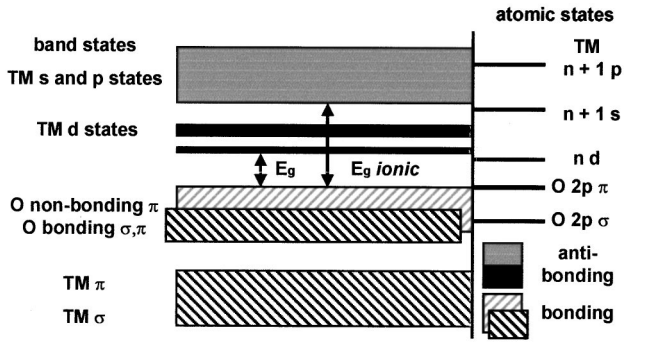

FIG. 2. Universal energy band diagram for transition metal/rare earth oxide dielectrics.

materials have been studied with far ultraviolet (UV) spectroscopic ellipsometry measurements and near-visible UV optical transmission measurements. The far UV spectroscopic ellipsometer used in these studies has a spectral scanning range extended from the conventional 6.5 eV limit up to 9 eV and thus is useful for the characterization of wide band gap bulk materials[9,10] as well as thin dielectric layers.[11]

II. EXPERIMENTAL EQUIPMENT: SPECTROSCOPIC ELLIPSOMETER

A far UV spectroscopic ellipsometer with rotating analyzer was built for characterization of materials including the high-*K* dielectrics of this study, as well as thin multilayer dielectric stacks and wide band gap semiconductors. Figure 1 shows a schematic of the far UV spectroscopic ellipsometer system. One of the most challenging requirements for a far UV measurement system is to operate the optical system in a UV-transparent ambient to avoid absorption by oxygen and its radicals that have absorption bands below about 190 nm. To accomplish this, the system was placed inside a glove box purged by dry nitrogen gas. All optical components were selected for far UV use including the deuterium lamp (3–9 eV) with a MgF_2 window, MgF_2 coated mirrors, MgF_2 Rochon prisms for polarizers, and a vacuum UV monochromator. In order to convert UV light to fluorescent light in the visible spectrum, the window of the photomultiplier tube (PMT) was coated by sodium salicylate;[12,13] this permits the use of a conventional PMT with a quartz window. A filter [maximum transmission of 37.2% at 161.4 nm; full width half maximum 52.20 nm] was placed between the vacuum UV monochromator and the focusing mirror to remove scattered light which otherwise distorts the signal in the wavelength range from 165 to 177 nm where the light intensity generated by the deuterium lamp and transmitted through the UV optical system is at a minimum. Details of the operation of the rotating analyzer ellipsometer have been described in previous publications.[14–16]

In this study, the ellipsometry measurements and transmission measurements were made on single crystals of $LaAlO_3$, Y_2O_3-stabilized HfO_2, $GdScO_3$, and $SmScO_3$. Details of the growth, crystallization, and dielectric characterizations of these crystals are published elsewhere.[17] Of these crystals, only $(Y_2O_3)_{0.15}-(HfO_2)_{0.85}$ is cubic; both $GdScO_3$ and $SmScO_3$ are orthorhombic, and $LaAlO_3$ is rhombohedral at room temperature. Note that the rhombohedral distortion of $LaAlO_3$ from cubic 0.1°[18] is slight. The optical measurements presented here were taken on (100) oriented $LaAlO_3$ (Ref. 19) and $GdScO_3$ crystals, and a direction-unspecified section of a smaller $SmScO_3$ crystal. The sample thicknesses were in the range of 0.5–1 mm. Ellipsometery parameters psi and delta (ψ and Δ, respectively) were measured in the spectral range from 3 to 9 eV. The measurements were performed from 3 eV; however, the data below about 4.8 eV were not considered in the extraction of real and imaginary parts of the complex dielectric function, $\epsilon_1 + i\epsilon_2$, because of the lack of accuracy in that spectral range. Second order scattered light from the higher photon energy region should not be a significant factor for wavelengths shorter than 300 nm (4 eV), as the deuterium lamp spectrum is relatively weak below about 150 nm. In addition to the ellipsometry measurements, transmission measurements were performed with a Perkin Elmer UV visible (VIS) spectrometer, Lambda 40. With the additional transmission data, it was anticipated that the band gap energy of high-*K* dielectrics could be determined more accurately than by the rotating-analyzer-based far UV spectroscopic ellipsometer measurement alone.

III. DATA ANALYSIS PROCEDURES

The intrinsic bulk dielectric response of samples was obtained from the ellipsometric measurements using a standard correction for surface roughness effects through the following simulation. The samples were modeled by a two-layer Bruggeman effective medium approximation in which the surface layer was approximated by a mixture of high-*K* dielectric and voids while the substrate was the pure high-*K* dielectric. The model was optimized to fit with ellipsometer and transmission data by varying the thickness and the composition of the surface layer; i.e., the effective optical path length of this surface layer.

Before presenting the data analysis for the crystals under study, it is important to establish a basis for the assignment of band gaps in these transition metal/rare earth oxide materials since these materials are qualitatively different from oxides free of transition metal and rare earth elements.[20,21] This also provides a framework for explaining and understanding the complementary nature of the information available from the VIS-UV optical absorption, and far UV ellipsometric measurements. Figure 2 shows the universal electronic structure for band edge states in transition metal/rare earth

TABLE I. Atomic energies of *nd* and $n+1s$ states of representative transition metal and rare earth elements, energy differences between the atomic *n d* and $n+1s$ states, as well as band gaps of some of the transition metal and rare earth oxides.

Element	Atomic *d* state (eV)	Atomic *s* state (eV)	Δ (*s*--*d* state energies) (eV)	Lowest optical band gap for elemental oxide
Sc	−9.35	−5.71	3.64	~4
Y	−6.80	−5.33	1.47	~6
La	−6.63	−5.42	1.21	~5–6
Gd	~6.6	~5.5	1.1	~5–6
Ti	−11.05	−6.04	5.01	3.1
Zr	−8.46	−5.67	2.79	5.5
Hf	−8.14	−5.71	2.43	5.8
Ta	−9.57	−5.97	3.60	4.4

oxides.[22] The validity of this scheme is well documented, for example a combination of x-ray absorption, x-ray emission, and electron energy loss spectroscopy has demonstrated that it provides a qualitative and quantitative description of the band edge electronic structure for crystalline TiO_2.[23] The highest occupied valence band states are derived from nonbonding oxygen atom 2*p* states with π character, and the lowest conduction bands, or antibonding states are derived from transition metal/rare earth atomic *d* states. The antibonding states occur as a doublet with a symmetry that reflects the coordination and bonding geometry of the transition metal/rare earth atom. Additionally, the individual components of these doublets can be split by the crystal symmetry and/or local site symmetry in which the transition metal/rare earth atom is in an off-center location as in ferroelectric perovskites. The *d* states are localized on the transition metal/rare earth atoms as demonstrated in Ref. 22, and have energy levels with respect to the valence band that scale with their respective *d*-state energies. The larger the *d*-state binding energy with respect to vacuum, the closer these *d* states lie to the oxygen atom derived valence band states. The lowest energy optical transition between the valence band and unoccupied transition metal/rare earth atom states involves the *d*-state derived conduction bands and is designated as E_g in Fig. 2. The next higher conduction bands in order of increasing energy are derived from antibonding *s* and *p* states of the transition metal/rare earth atoms. This band gap is designated as the E_g ionic in Fig. 2. Transitions between the valence band and this higher conduction band are similar in character to the band gap transitions in nontransition metal/rare earth oxides such as noncrystalline SiO_2 and Al_2O_3, and the effective band gaps are in the same general energy range of 7–10 eV.[22] In some of the measurements that follow, the VIS-UV absorption data reveal the lowest band gap transitions associated with the *d* states, whilst the UV-ellipsometric measurements reveal the onset of on excitations associated with the transition metal/rare earth atom *s* states.

Table I lists the energies of the atomic *nd* and $n+1$ *s* states of transition metals and rare earth elements that are important for the analysis of the spectroscopic data. Pervious studies have demonstrated that the lowest band gaps of transition metal oxides scale in direct proportion to the atomic *d*-state energies; i.e., the lower the *d*-state energy with respect to vacuum, the smaller the band gap of transition metal oxide.[22] Table I also includes experimentally determined band gaps for some of the materials listed. The *intra conduction* band gap between the *d* state bands and the conduction band derived from the transition metal/rare earth *s* states has been found to scale with the difference between the energies of the $n+1$ *s* and *n d* states.

IV. EXPERIMENTAL RESULTS AND INTERPRETATION OF DATA

Figure 3 is the transmission spectrum of $LaAlO_3$. It shows that the optical transmission starts at about 5.5 eV. There are no sharp features in this spectrum that can be assigned to transitions involving *d* states. This is consistent with the band structure of Fig. 2 in which the atomic *d* states of La are relatively high in energy, and close to the La atom *s* states. This means that the energy separation between E_g and E_g ionic band gaps is expected to be small for La_2O_3. Consider next the ellipsometric data and the extraction of the complex dielectric constant, $\epsilon_1 + i\epsilon_2$. For $LaAlO_3$, the best fit extraction was obtained with a 17 Å thick surface layer with an 80% void fraction. Figure 4 shows the dielectric functions ϵ_1 and ϵ_2 of a $LaAlO_3$ single crystal that resulted from the simulation algorithm. First, this simulation demonstrates that the peaks of real and imaginary parts of the complex dielectric constant, ϵ_1 and ϵ_2, respectively, for $LaAlO_3$ occur well above 6.5 eV, which is the upper limit of most conventional ellipsometers. The variation in the peak height

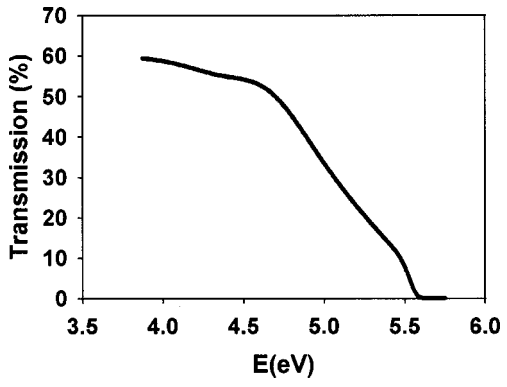

FIG. 3. Transmission spectrum of a $LaAlO_3$ single crystal.

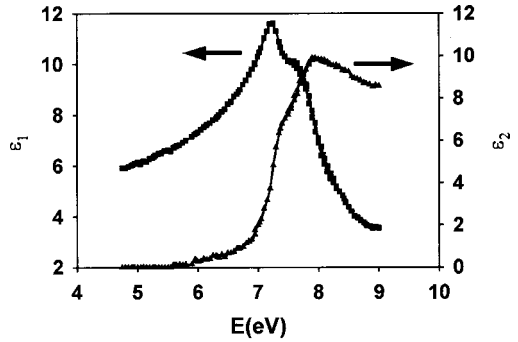

FIG. 4. Dielectric functions ϵ_1 and ϵ_2 of a $LaAlO_3$ single crystal.

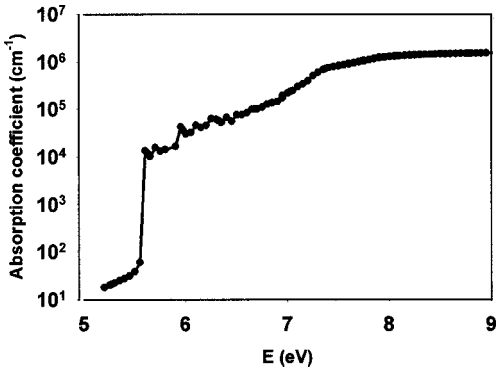

FIG. 5. Absorption coefficient of a $LaAlO_3$ single crystal as a function of photon energy.

and shape of these features additionally provides information that can be correlated with the surface and material quality.[10,24]

In the context of the band diagram of Fig. 2, the steep rise in ϵ_2 at about 7 eV is assigned to the ionic gap (see Tables I and II). Next, in order to find the lowest optical band gap of $LaAlO_3$ associated with the *d*-state transitions, the dielectric functions ϵ_1 and ϵ_2 were converted to a complex index of refraction, $n+ik$. The absorption coefficient α was then calculated from the equation

$$\alpha = \frac{4\pi k}{\lambda}, \tag{1}$$

where k is the imaginary component of the complex refractive index and λ is the wavelength in units of cm. Figure 5 is a semilog plot of the absorption coefficient α versus photon energy. The steep increase in α approximately defines the lowest absorption edge as expected for a direct band gap material.[25] In this instance, it is characteristics of an exciton-like band edge feature associated with the La *d* states. The structures between about 5.5 and 6.0 eV are tentatively assigned to departures from isotropic symmetry, i.e., the rhombohedral distortion noted above. These will remove the degeneracies in the *d* band features. A striking example of this will be discussed below with respect to the absorption spectra of $SmScO_3$.

The energy difference of about 1.4 eV between the first of these *d* bands, and the onset of stronger absorption associated with antibonding *s* states of La is consistent with the relatively small difference between the atomic *s* and *d* states of La, ~1.2 eV (see Table I). This threshold energy for absorption is evident in the ϵ_2 spectrum in Fig. 4, as well as in the calculated absorption constant in Fig. 5.

For the Y_2O_3-stabilized HfO_2, the transmission measurement shows that the cutoff wavelength is about the same as of $LaAlO_3$ and thus, the effective optical band gap for *d*-band absorption of HfO_2 is expected to be very close to that of $LaAlO_3$, ~5.8 eV, in agreement with a previous determination of the band gap from the threshold for photoconductivity, ~5.8 eV.[26] The simulation of HfO_2 to extract the real and imaginary parts of the complex dielectric function was also performed using a two-layer Bruggeman effective medium approximation. The derived surface layer has 41 Å thickness and 61% void fraction. Figure 6 shows the resulting dielectric functions ϵ_1 and ϵ_2 for single crystal HfO_2. Relative to the dielectric functions of $LaAlO_3$, the ϵ_1 peak of HfO_2 is located at a slightly lower energy of approximately 6.7 eV, but there is no distinct ϵ_2 peak up to a photon energy of 9 eV. In addition, there is no spectroscopic evidence for the doublet *d*-state bands that have been reported in ZrO_2 based on x-ray absorption spectroscopy (XAS).[27] This is consistent with XAS measurements performed on HfO_2 thin films, where the doublet components are significantly broader than for ZrO_2, ~7 eV and compared to <2 eV for ZrO_2, and where the splitting is significantly greater, ~10 eV as compared to <4 eV for ZrO_2.[28] The ionic gap is estimated to be about 6.8 eV. The point of steepest slope in the ϵ_2 plot and the separation between the ionic gap and the onset of strong absorption is then about 1 eV, which is less than the Hf $6s-4d$ atomic energy separation, but consistent with the increased width of the *d*-band doublet as observed in the XAS study.

The transmission spectrum of $GdScO_3$ is shown in Fig. 7. Unlike the other materials discussed above, this spectrum shows considerable sub-band gap absorption that will be in-

TABLE II. Summary of experimental results from this study.

Oxide	*s*-state band gap (eV)	*d*-state band gaps (eV)	Average intra conduction band gap (eV)	Δ (*s*--*d*-state energies) (eV)
$LaAlO_3$	7.0	5.6,6.0(La)	1.2	1.21
HfO_2	6.8	~5.8	1.0	2.43
$GdScO_3$	6.5	3.9,4.4,4.9(Sc)	2.1	3.64
$SmScO_3$	~6	...	...	...

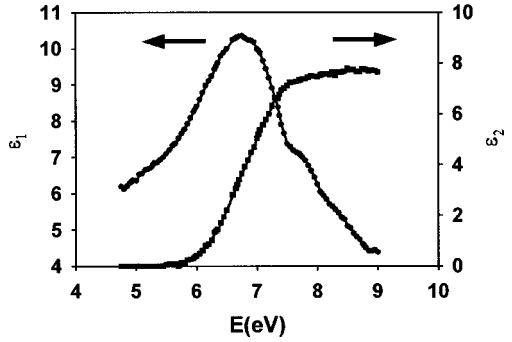

FIG. 6. Dielectric functions ϵ_1 and ϵ_2 of a yttria-stabilized HfO_2 single crystal.

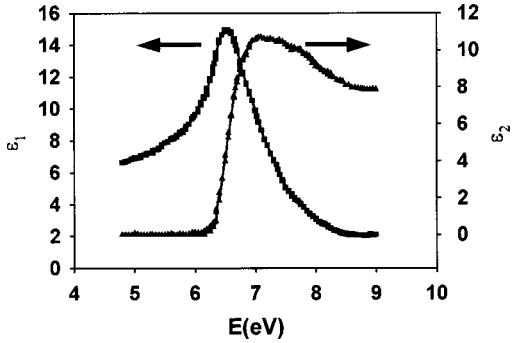

FIG. 8. Dielectric functions ϵ_1 and ϵ_2 of a $GdScO_3$ single crystal.

terpreted in terms of the electronic structure of transition metal insulating elementary and binary oxides. The sharp absorption in Fig. 7 are consistent with the universal energy band scheme of Fig. 2. Based on comparisons with XAS,[28] these three bands ~3.9, 4,4, and 4.9 eV, are the crystal symmetry split features of a transition metal *d* state. The three features are consistent with the orthorhombic crystal structure, and the additional splitting of each feature is consistent with the fact that the Sc atom is off center in the perovskite structure.

The dielectric functions of the $GdScO_3$ substrate were obtained as described above, and are shown in Fig. 8. In the simulation step, a 19.5 Å thick top layer with 20.3% void fraction was employed. The sub-band gap features of Fig. 7 in the transmission measurement do not show up in this analysis of the ellipsometric data. This is understood from the following argument. The dielectric functions ϵ_1 and ϵ_2 are related to the complex index of refraction *n* and *k* by the following equations: $\epsilon_1 = n^2 - k^2$ and $\epsilon_2 = 2nk$. Below the band gap, the imaginary component of the index of refraction *k* is very close to 0, therefore, the above equations approximate to $\epsilon_1 \sim n^2$ and $\epsilon_2 \sim 0$. Since $\epsilon_2 \sim 0$, the variation in ϵ_2 is too small to detect ellipsometrically and is therefore no observable in Fig. 8. On the other hand, since the absorption coefficient is $\alpha = 4\pi k/n$, we do not expect transmission measurements to directly impact our least squares fit to *n* and therefore to $\epsilon_1 \sim n^2$. Consequently, the variation in ϵ_1 is not observable.

The spectral dependence of the absorption coefficient of $GdScO_3$ in the strongly absorbing region was next calculated by Eq. (1) using the extracted dielectric functions of Fig. 8. The band gap energy estimated is this way is approximately 6.5 eV. If this band edge is associated with the *s* band of Sc, then the separation between 3d and 4*s* states of Sc is estimated to be ~2.6 eV, less than the atomic spacing of >3.5 eV (see Table I).

For $SmScO_3$, only ellipsometry data were used in the analysis since the transmission measurement with the UV/VIS spectrometer was not successful for the small sample used (diameter ~3 mm). Figure 9 shows the dielectric function of $SmScO_3$ extracted after the simulation. It is observed that the tail of the ϵ_2 spectrum does not go to zero as is in the case of $GdScO_3$ in Fig. 8. This may be due in part to scattered light in this energy range; we therefore extrapolate a band gap from the steepest part of the ϵ_2 higher energy results. Again, the band gap energy estimated in this way is between 5.5 and 6.0 eV, and consistent with the atomic state energies of Sm and Sc. Table II includes a summary of the optical band gap measurements for these four high-*K* dielectrics.

V. CONCLUSIONS

In summary, we built a far UV spectroscopic ellipsometer system and investigated the single crystal optical properties of four high-*K* dielectrics: $LaAlO_3$, Y_2O_3 stabilized HfO_2, $GdScO_3$, and $SmScO_3$. This was by a combination of UV ellipsometry measurements and UV/VIS optical transmission measurements. The complex dielectric functions of

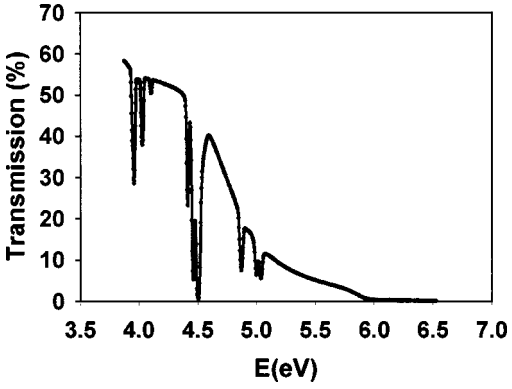

FIG. 7. Transmission spectrum of a $GdScO_3$ single crystal.

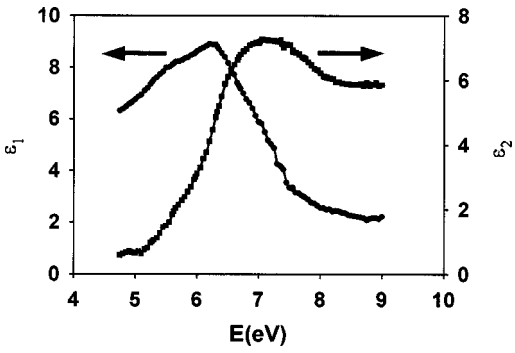

FIG. 9. Dielectric functions ϵ_1 and ϵ_2 of a $SmScO_3$ single crystal.

these materials were determined to be from 4.75 to 9 eV. Optical band gaps were estimated from the transmission and ellipsometric studies. Based on the energy band scheme of Fig. 2, it is necessary to specify more than one optical band gap. The lowest band gap energies are associated with *d* states of the transition metal atoms La, Hf, and Sc and the rare earth atoms Gd and Sm. An ionic band gap at higher energy is associated with transitions that terminate in transition metal or rare earth atom *s* dates. Finally, it has been shown that far UV spectroscopic ellipsometry with extended spectral energy is a promising tool for studies of high-*K* dielectric materials.

ACKNOWLEDGMENTS

D.G.S., J.H.H., and G.L. gratefully acknowledge the financial support of the Semiconductor Research Corporation (SRC) and SEMATECH through the SRC/SEMATECH FEP Center. J.H.H. gratefully acknowledges a Motorola/SRC Fellowship. G.L. is also supported in part by the Office of Naval Research (ONR) and the Air Force Office of Scientific Research (AFOSR). The authors also thank Guenther Appel for sharing his unpublished XAS results, Frank Lichtenburg of Augsburg University for help with the floating zone apparatus (supported by the BMBF through Project No. 13N6918/1), and Susan Trolier-McKinstry for helpful discussions.

[1] T. H. DiStefano and D. E. Eastman, Solid State Commun. **9**, 2259 (1971).
[2] M. L. Green, T. W. Sorsch, G. L. Timp, D. A. Muller, B. E. Weir, P. J. Silverman, S. V. Moccio, and Y. O. Kim, Microelectron. Eng. **48**, 25 (1999).
[3] W. Qi, B.H. Lee, R. Nieh, L. Kang, Y. Jeon, K. Onishi, and J. C. Lee, Proc. SPIE **3881**, 24 (1999).
[4] K. J. Hubbard and D. G. Schlom, J. Mater. Res. **11**, 2757 (1996).
[5] C. A. Billman, P. H. Tan, K. J. Hubbard, and D. G. Schlom, Mater. Res. Soc. Symp. Proc. **567**, 409 (1999).
[6] D. G. Schlom, C. A. Billman, J. H. Haeni, J. Lettieri, P. H. Tan, R. R. M. Held, S. Völk, and K. J. Hubbard, Appl. Phys. A: Mater. Sci. Process (to be published).
[7] D. G. Schlom and J. H. Haeni, MRS Bull. (to be published).
[8] J-P. Maria, W-H. Schulte, D. Wicaksana, B. Busch, A. I. Kingon, and E. Garfunkel (unpublished).
[9] C. Cobet, K. Wilmers, T. Wethamp, N. V. Edwards, N. Esser, and W. Richter, Thin Solid Films **364**, 111 (2000).
[10] S. Lim, T. N. Jackson, W. C. Mitchel, R. Bertke, and J. L. Freeouf, Appl. Phys. Lett. **79**, 162 (2001).
[11] J. L. Freeouf, US Patent No. 6,222,199 B1.
[12] M. Seya and F. Masuda, Sci. Light (Tokyo) **12**, 9 (1963).
[13] J. A. R. Samson, *Technqiues of Vacuum Ultraviolet Spectroscopy* (Wiley, New York, 1967), Chap. 7.
[14] D. E. Aspnes, J. Opt. Soc. Am. **64**, 639 (1974).
[15] D. E. Aspnes and A. A. Studna, Appl. Opt. **14**, 220 (1975).
[16] R. W. Collins, Rev. Sci. Instrum. **61**, 2029 (1990).
[17] J. H. Haeni, S. Trolier-McKinstry, D. G. Schlom, S. Lim, T. N. Jackson, M. M. Rosario, J. L. Freeouf, R. Uecker, and P. Reiche (unpublished).
[18] *Landolt-Börnstein: Numerical Data and Functional Relationships in Science and Technology*, edited by K.-H. Hellwege and A. M. Hellwege, New Series, Group III, Vol. 7d2 (Springer, Berlin, 1980), p. 179.
[19] Pseudocubic indices. For the rhombohedral axes, the $LaAlO_3$ orientation is (110).
[20] J. Robertson and C. W. Chen, Appl. Phys. Lett. **74**, 1164 (1999).
[21] J. Robertson, J. Vac. Sci. Technol. B **18**, 1785 (2000).
[22] G. Lucovsky, J. L. Whitten, and Yu Zhang, Microelectron. Eng. **59**, 329 (2001).
[23] P. A. Cox, *Transition Metal Oxides* (Oxford Science, Oxford, 1992).
[24] C. A. Richter, N. V. Nguyen, and G. B. Alers, Mater. Res. Soc. Symp. Proc. **567**, 559 (1999).
[25] J. M. Essick and R. T. Mather, Am. J. Phys. **61**, 646 (1993).
[26] S. Campbell and V. V. Anfanasv'ev (unpublished).
[27] G. Lucovsky, G. B. Rayner, D. Kang, G. Appel, R. S. Johnson, Y. Zhang, D. E. Sayers, and J. L. Whitten, Appl. Phys. Lett. **79**, 1775 (2001).
[28] G. Appel, J. G. Hong, and G. Lucovsky (unpublished).